Supplementary Information for Novel two-dimensional β-GeSe and β-SnSe semiconductors: anisotropic high carrier mobility and excellent photocatalytic water splitting

Yuanfeng Xu,*[a] Ke Xu,[b] Congcong Ma,[c] Ying Chen,[c] Hao Zhang,*[b] Yifan Liu,[a] and Yanju Ji[a]

[a] School of Science, Shandong Jianzhu University, Jinan 250101, Shandong, China.

[b] Key Laboratory for Information Science of Electromagnetic Waves (MoE),

Key Laboratory of Micro and Nano Photonic Structures

(MoE) and Department of Optical Science and Engineering,

Fudan University, Shanghai 200433, China.

[c] Academy for Engineering and Technology, Fudan University,

and Engineering Research Center of Advanced Lighting Technology,

Ministry of Education, Shanghai 200433, China. and

Correspondence: xuyuanfeng19@sdjzu.edu.cn (Yf. Xu); zhangh@fudan.edu.cn (H. Zhang)
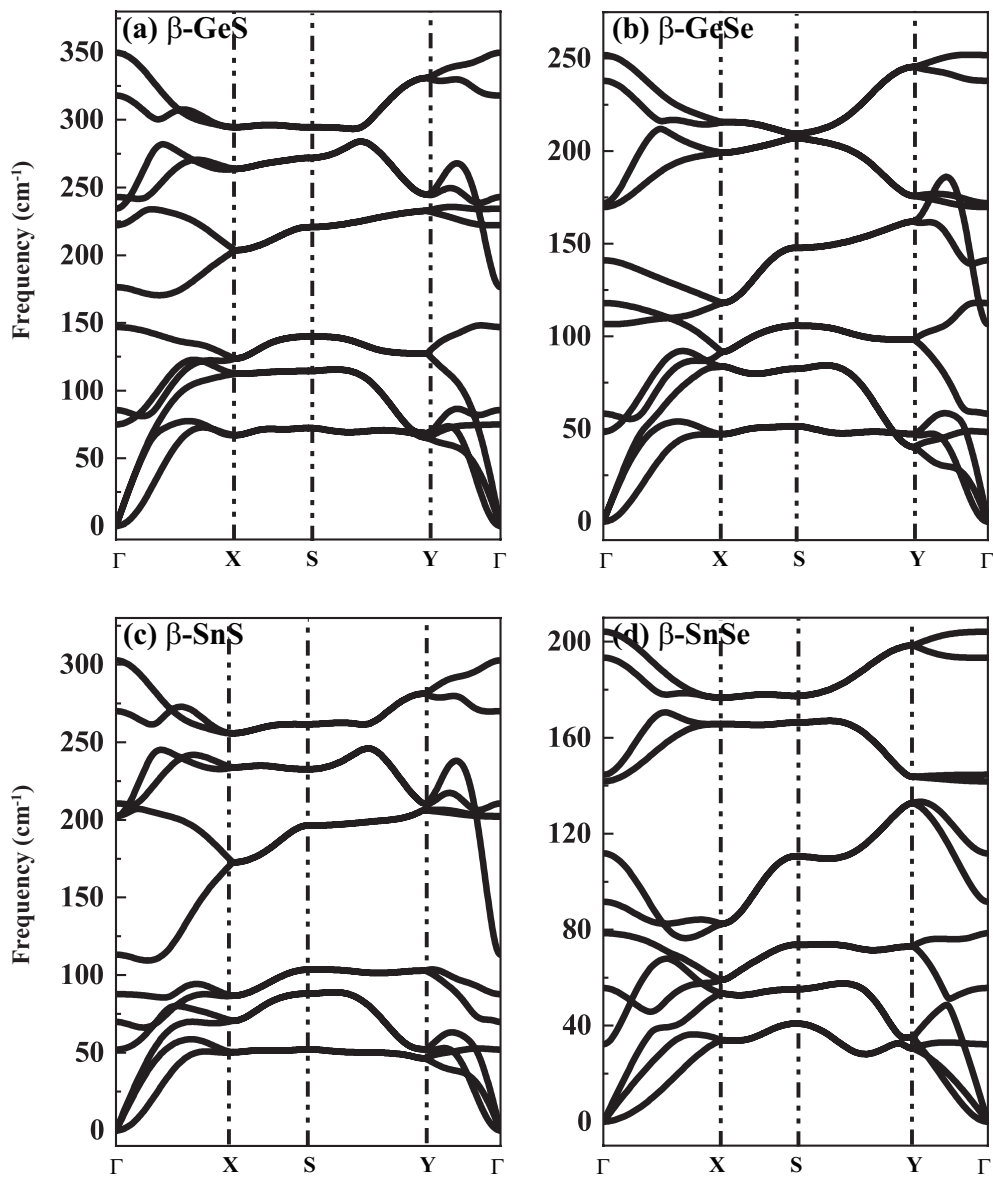
1. The phonon spectrum for monolayer β-MX

FIG. S1: The calculated phonon dispersions for monolayer (a) β-GeS, (b) β-GeSe, (c) β-SnS and (d) β-SnSe

2. PBE and HSE06 calculated band structure of monolayer group-IV monochalcogenides: β-GeS, β-GeSe, β-SnS and β-SnSe
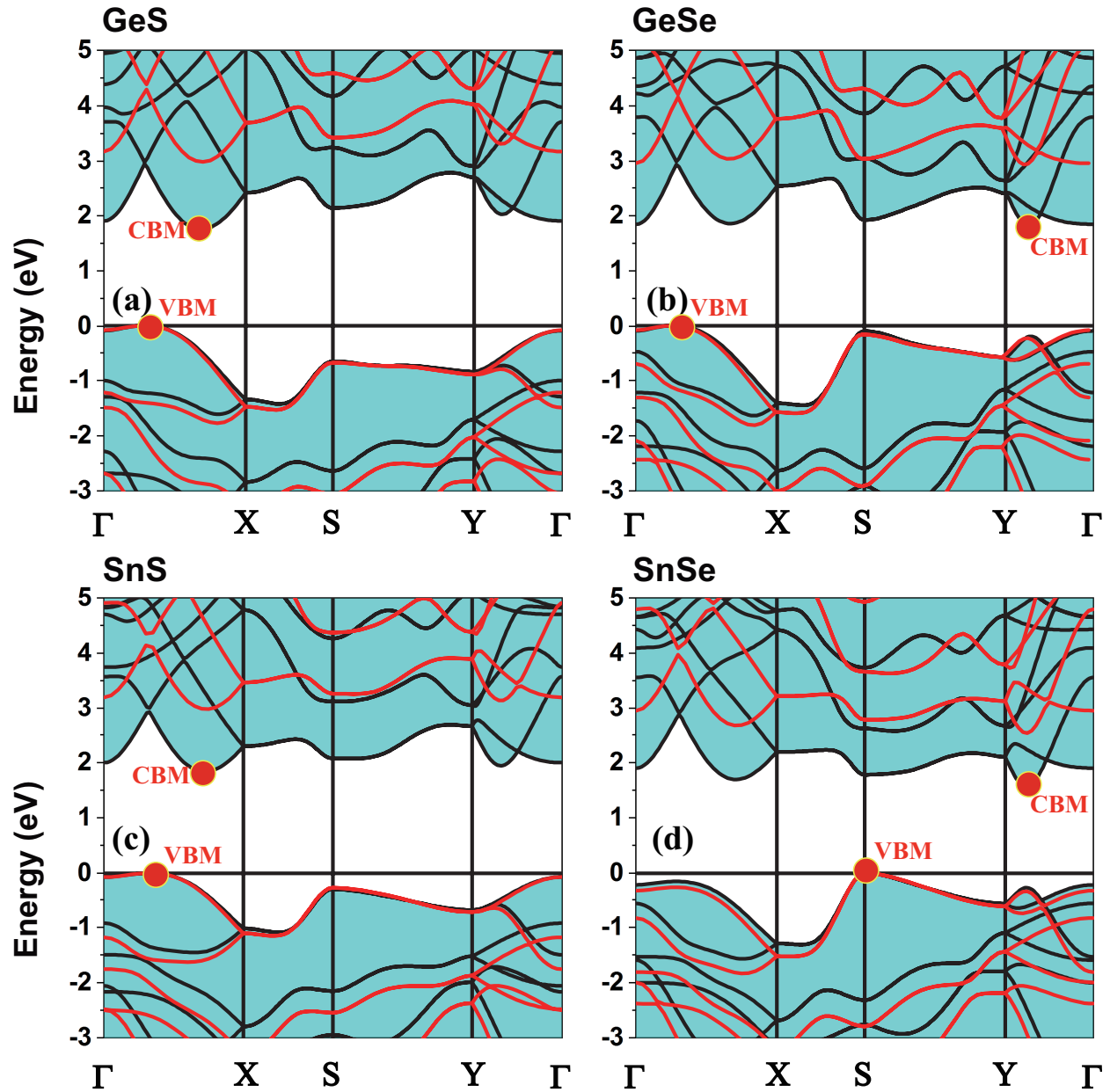
FIG. S2: Band structures of (a) β-GeS, (b) β-GeSe, (c) β-SnS and (d) β-SnSe monolayers. Black and red lines respectively indicate the band structures based on PBE and HSE06 levels. The fermi levels are set to 0 eV.

3. Computational details of carrier mobility of 2D materials

The intrinsic carrier mobilities μ^{2D} of $\beta-$phase group-IV monochalcogenides, i.e. β-GeS, β-GeSe, β-SnS and β-SnSe, are calculated by using the deformation potential theory, which was proposed by Bardeen and Shockley[1] in 1950s to describe the charge transport property for non-polar semiconductors. Due to the large electron wavelength (about 7 nm) corresponding to the lattice constant and bond length, longitudinal phonon scattering dominates the intrinsic mobility transport properties of nonpolar 2D materials. The carrier mobility based on the deformation potential theory for 2D systems is given by[2, 3],

$$\mu^{2D} = \frac{e\hbar^3 C_{2D}}{k_B T m^* m_d E_d^2},\tag{1}$$

where e is the electron charge, $\hbar$ is the reduced Planck's constant, T is the temperature equal to 300 K throughout the paper. C_{2D} is the elastic modulus of a uniformly deformed crystal by strains and derived from $C_{2D} = [\partial^2 E/\partial^2 (\Delta l/l_0)]/S_0$, in which E is the total energy, Δl is the change of lattice constant l_0 along the transport direction, and S_0 represents the lattice volume at equilibrium for a 2D system. The effective mass m^* of holes (m_h^*) and electrons (m_e^*) along the transport direction are obtained by fitting parabolic functions to the VBM and CBM, respectively, and given by $m^* = \hbar^2 (\partial^2 E(k)/\partial k^2)^{-1}$ (k is wave-vector, and $E(k)$ denotes the energy) (either m_x^* or m_y^* along the x or y direction, respectively), m_d is the average effective mass defined by $m_d = \sqrt{m_x^* m_y^*}$. E_d is the deformation potential (DP) constant defined by $E_d^{e(h)} = \Delta E_{CBM(VBM)}/(\Delta l/l_0)$, where $\Delta E_{CBM(VBM)}$ is the energy shift of the band edge with respect to the vacuum level under a small dilation Δl of the lattice constant l_0.

4. Strain-shifts of VBM and CBM, strain-total energy relations under uniaxial strain along x and y directions for monolayer $\beta-$GeS, $\beta-$GeSe, $\beta-$SnS and $\beta-$SnSe

FIG. S3: Dependence of band edges (VBM and CBM) with respect to vacuum as a function of applied uniaxial strains along the x (a) and y (b) directions for monolayer β-GeS. (c) The relationship between the total energy and strain along the x and y directions.
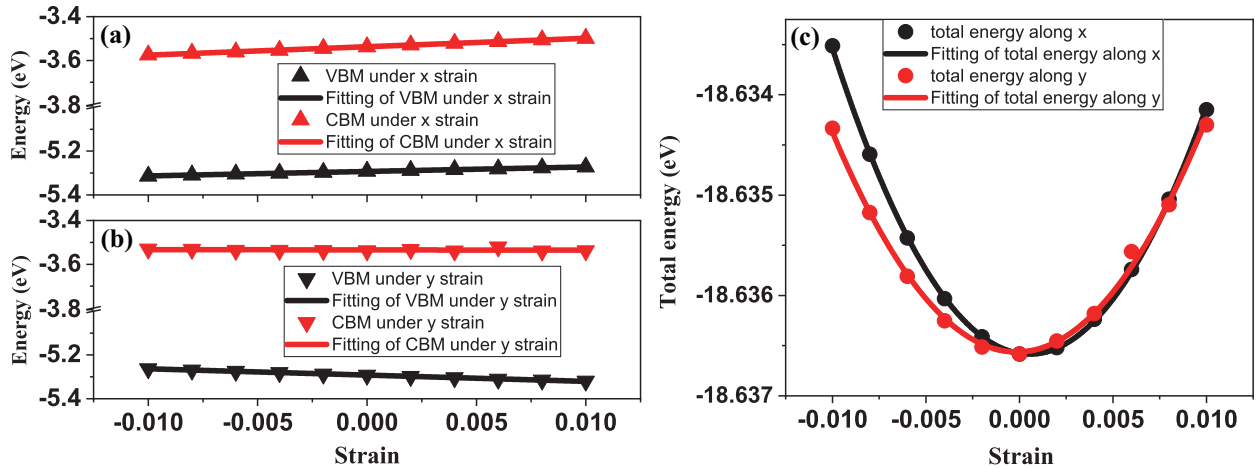

FIG. S4: Dependence of band edges (VBM and CBM) with respect to vacuum as a function of applied uniaxial strains along the x (a) and y (b) directions for monolayer β-GeSe. (c) The relationship between the total energy and strain along the x and y directions.
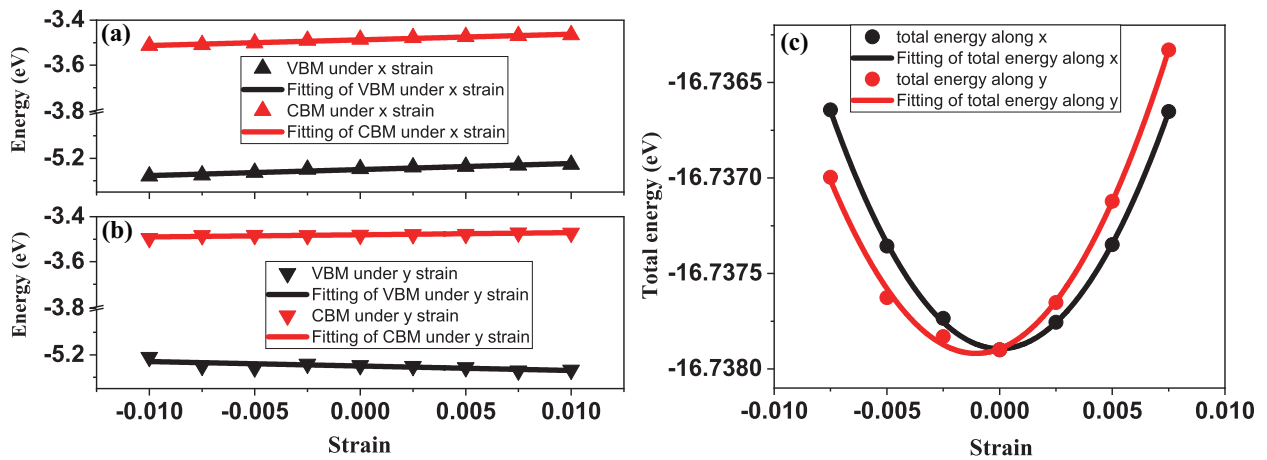
FIG. S5: Dependence of band edges (VBM and CBM) with respect to vacuum as a function of applied uniaxial strains along the x (a) and y (b) directions for monolayer β-SnS. (c) The relationship between the total energy and strain along the x and y directions.
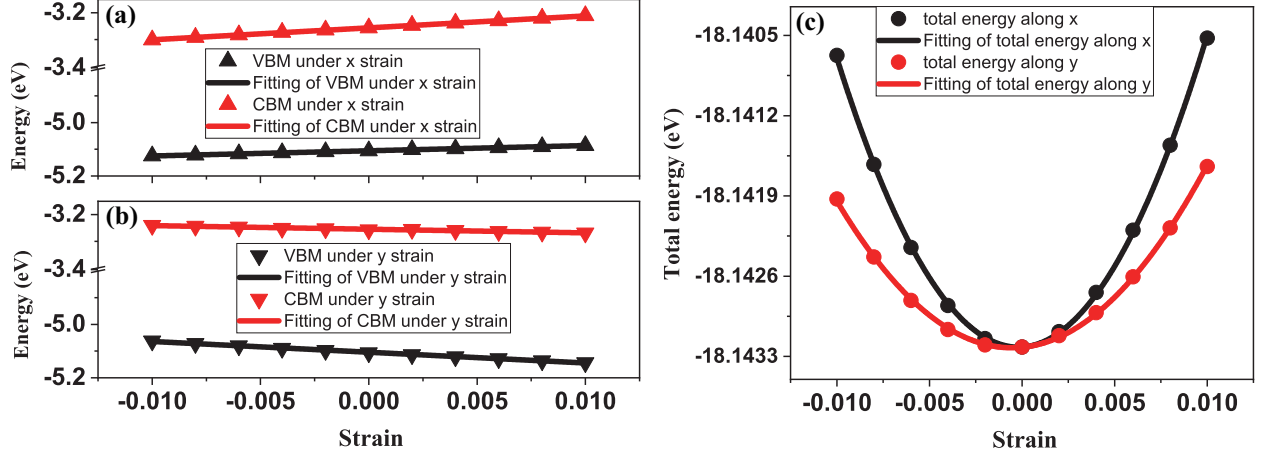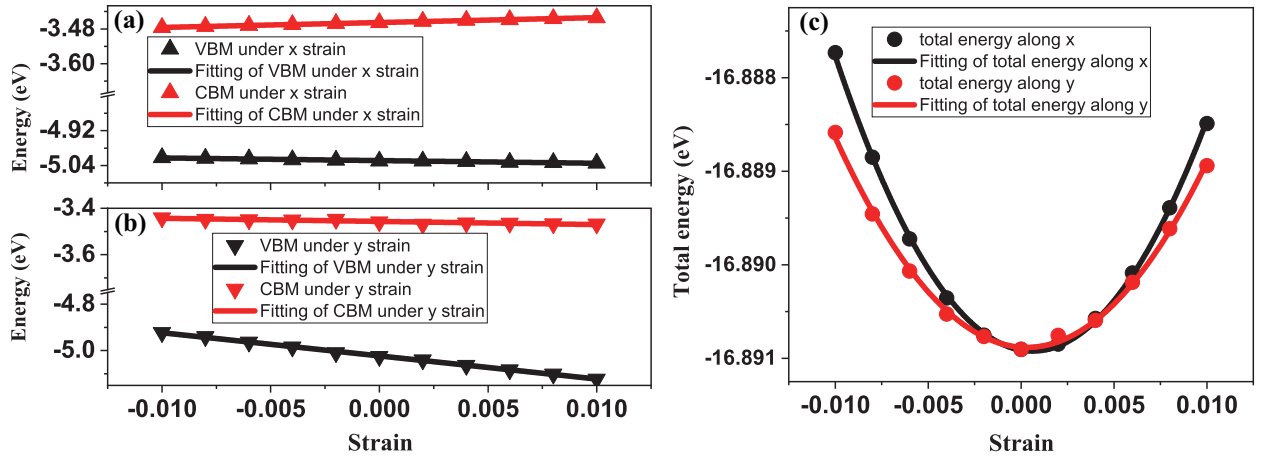

FIG. S6: Dependence of band edges (VBM and CBM) with respect to vacuum as a function of applied uniaxial strains along the x (a) and y (b) directions for monolayer β-SnSe. (c) The relationship between the total energy and strain along the x and y directions.

5. Thermodynamic oxidation and reduction potentials of β-GeSe and β-SnSe monolayers in aqueous solution

According to the previous literature[4, 5], the monolayer β-GeSe and β-SnSe can be reduced by the photogenerated electrons through the following reaction:

$$Ge_2Se_2/Sn_2Se_2 + 2H_2 \rightarrow 2Ge/Sn + 2H_2Se \tag{2}$$

6
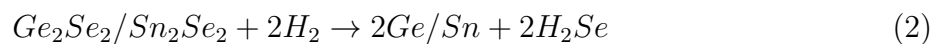
The thermodynamic reduction potential of monolayer β-GeSe and β-SnSe ($\phi^{re-GeSe/SnSe}$) could be calculated as following:

$$\phi^{re-GeSe/SnSe} = -[2\Delta_f G^0(Ge/Sn) + 2\Delta_f G^0(H_2Se) - \Delta_f G^0(GeSe/SnSe) - 2\Delta_f G^0(H_2)]/4eF + \phi(H^+/H_2) \tag{3}$$

where $\Delta_f G^0(Ge)$, $\Delta_f G^0(Sn)$, $\Delta_f G^0(H_2Se)$, $\Delta_f G^0(GeSe/SnSe)$ and $\Delta_f G^0(H_2)$ denote the standard molar Gibbs energy of formation of Ge, Sn, H_2Se, GeSe/SnSe and H_2. As listed in Table S1, the $\Delta_f G^0(Ge)$, $\Delta_f G^0(Sn)$, $\Delta_f G^0(H_2Se)$ and $\Delta_f G^0(H_2)$ could be found in the handbook[6]. The standard molar Gibbs energy of formation of β-GeSe and β-SnSe are approximated by their formation energy (E_{f-GeSe} and E_{f-SnSe}) [5], which is defined as follows:

$$E_{f-GeSe/SnSe} = E_{GeSe/SnSe} - 2E_{Ge/Sn} - 2E_{Se} \tag{4}$$

where $E_{GeSe/SnSe}$ means the total energy of β-GeSe and β-SnSe, while $E_{Ge/Sn}$ and E_{Se} denote the energies of Ge, Sn and Se in their stable phases respectively. E_{Ge}, E_{Sn} and E_{Se} are -4.03, -4.01 and -3.49 eV/atom, respectively. The total energy of β-GeSe and β-SnSe are -16.74 and -16.89 eV/unit. Therefore, the formation energy of β-GeSe (E_{f-GeSe}) and β-SnSe (E_{f-SnSe}) are -1.70 and -1.89 eV/unit. $\phi(H^+/H_2)$ is 0 V relative to the normal hydrogen electrode (NHE) potential. F and e represent the Faraday constant and the elemental charge, respectively. According to Equation (3), $\phi^{re-GeSe}$ and $\phi^{re-SnSe}$ are obtained as -2.23 and -1.94 V (relative to NHE), both higher than the $\phi(H^+/H_2)$ (0 V relative to NHE). Therefore, both β-GeSe and β-SnSe can be resistant against the reduction by the photo-excited electrons.

Furthermore, the β-GeSe and β-SnSe can be oxidize by the photogenerated holes through the following reaction:

$$Ge_2Se_2/Sn_2Se_2 + 2H_2O \rightarrow 2Se + 2GeO/SnO + 2H_2 \tag{5}$$

The thermodynamic oxidation potential of monolayer β-GeSe and β-SnSe ($\phi^{ox-GeSe/SnSe}$) could be calculated as following:

TABLE S1: Standard molar Gibbs energy of formation $(\Delta_f G^0)$[6] at 298.15 K in kJ/mol.

Molecular Formula	$\Delta_f G^0$	Molecular Formula	$\Delta_f G^0$
Ge	331.2	H_2O	-237.1
Sn	266.2	GeO	-73.2
Se	187	SnO	-126.4
H_2	0	H_2Se	15.9

$$\phi^{ox-GeSe/SnSe} = [2\Delta_f G^0(Se) + 2\Delta_f G^0(GeO/SnO) + 2\Delta_f G^0(H_2) - \Delta_f G^0(GeSe/SnSe)$$
$$-2\Delta_f G^0(H_2O)]/4eF + \phi(H^+/H_2) \quad (6)$$

where $\Delta_f G^0(Se)$, $\Delta_f G^0(GeO/SnO)$ and $\Delta_f G^0(H_2O)$ denote the standard molar Gibbs energy of formation of Se, GeO/SnO and H_2O. As listed in Table S1, the $\Delta_f G^0(Se)$, $\Delta_f G^0(GeO/SnO)$ and $\Delta_f G^0(H_2O)$ could be found in the handbook[6]. According to Equation (6), $\phi^{ox-GeSe}$ and $\phi^{ox-SnSe}$ are obtained as 2.25 and 2.02 V (relative to NHE), both lower than the $\phi(O_2/H_2O)$ (1.23 V relative to NHE). Therefore, both β-GeSe and β-SnSe can be resistant against the oxidation by the photo-excited holes.

6. Computational details of free energy change (ΔG) of monolayer β-GeSe and β-SnSe

We have systematically investigated the reaction pathways of both water oxidation and hydrogen reduction of monolayer β-GeSe and β-SnSe as shown in Fig.8, and the computational details are presented as follows,

To compute the free energy change (ΔG) in the hydrogen reduction and water oxidation reactions, we adopted the method developed by Norskov et al.[7], according to which the ΔG of an electrochemical reaction is computed as

$$\Delta G = \Delta E + \Delta E_{zpe} - T\Delta S + \Delta G_{pH} + \Delta G_U \quad (7)$$

where ΔE is the adsorption energy, ΔE_{zpe} and ΔS are the difference in zero point energy and entropy difference between the adsorbed state and the gas phase, respectively. The
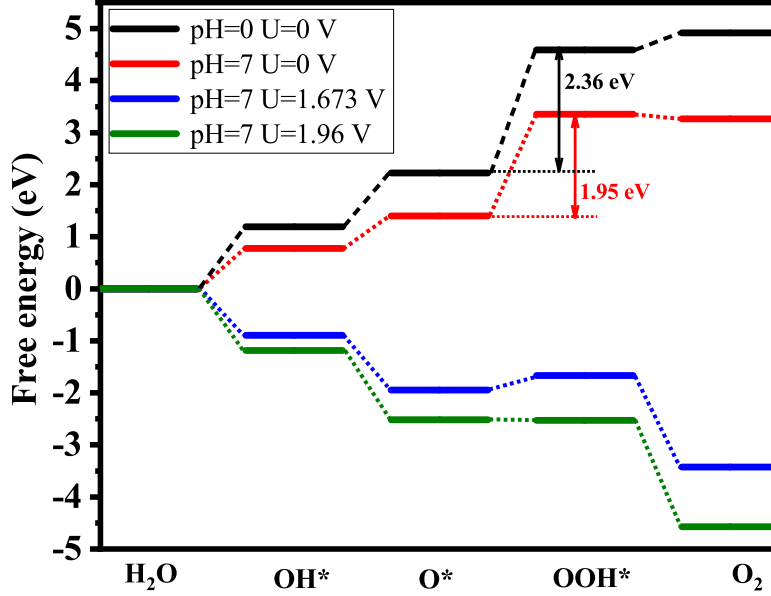
FIG. S7: The free energy steps of oxygen evolution reaction of monolayer β-SnSe under different conditions.

entropies of free molecules can be found from the NIST database[8]. T represents indoor temperature in this work. ΔG_{pH} ($\Delta G_{pH} = k_B T \times ln10 \times pH$) represents the free energy contributed in different pH concentration. ΔG_U (ΔG_U=-eU) denotes extra potential bias provided by an electron in the electrode, where U is the electrode potential relative to the standard hydrogen electrode (SHE).

There are four steps to transform H_2O into O_2 molecule in oxidation half reaction, which can be written as:

$$* + H_2O \rightarrow OH^* + H^+ + e^- \tag{8}$$

$$OH^* \rightarrow O^* + H^+ + e^- \tag{9}$$

$$O^* + H_2O \rightarrow OOH^* + H^+ + e^- \tag{10}$$

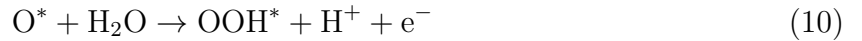$$OOH^* \rightarrow^* + O_2 + H^+ + e^- \tag{11}$$

9

TABLE S2: Total energy (E), zero-point energy correction (E_{zpe}), entropy contribution (TS, T=298.15K) and the Gibbs free energy (G) of molecules and adsorbates in β-GeSe system.

Species	E (eV)	$E_{zpe}(eV)$	-TS (eV)	G (eV)
H_2	-6.77	0.27	-0.41	-6.91
H_2O	-14.22	0.56	-0.67	-14.33
OH*	-76.80	0.34	-0.11	-76.56
O*	-72.72	0.06	-0.08	-72.74
OOH*	-80.86	0.43	-0.21	-80.64
H*	-69.09	0.11	-0.02	-69.00

Meanwhile, the hydrogen production half reaction can be decomposed into two steps, and the reaction equation can be written as:

$$* + H^+ + e^- \rightarrow H^* \tag{12}$$

$$*H + H^+ + e^- \rightarrow^* + H_2 \tag{13}$$

where $*$ means the adsorbed materials, O^*, OH^*, H^* and OOH^* represent the adsorbed intermediates.

For each reaction of both oxidation and hydrogen production, the free energy difference under the effect of pH and an extra potential bias can be written as:

$$\Delta G_1 = G_{OH^*} + \frac{1}{2}G_{H_2} - G_* - G_{H_2O} + \Delta G_U - \Delta G_{pH} \tag{14}$$

$$\Delta G_2 = G_{O*} + \frac{1}{2}G_{H_2} - G_{OH^*} + \Delta G_U - \Delta G_{pH} \tag{15}$$

$$\Delta G_3 = G_{OOH*} + \frac{1}{2}G_{H_2} - G_{O*} - G_{H_2O} + \Delta G_U - \Delta G_{pH} \tag{16}$$

$$\Delta G_4 = G_* + \frac{1}{2}G_{H_2} + G_{O_2} - G_{OOH^*} + \Delta G_U - \Delta G_{pH} \tag{17}$$

$$\Delta G_5 = G_{H^*} - \frac{1}{2}G_{H_2} - G_* + \Delta G_U + \Delta G_{pH} \tag{18}$$

$$\Delta G_6 = G_* + \frac{1}{2}G_{H_2} - G_{H*} + \Delta G_U + \Delta G_{pH} \tag{19}$$

It should be noted that in this approach no explicit photoexcitation is described, but the effect of photo-generated electrons is included via the shift of the individual reaction free

10

TABLE S3: Total energy (E), zero-point energy correction (E_{zpe}), entropy contribution (TS, T=298.15K) and the Gibbs free energy (G) of molecules and adsorbates in β-SnSe system.

Species	E (eV)	$E_{zpe}(eV)$	-TS (eV)	G (eV)
H_2	-6.77	0.27	-0.41	-6.91
H_2O	-14.22	0.56	-0.67	-14.33
OH*	-74.33	0.33	-0.12	-74.13
O*	-69.61	0.06	-0.09	-69.64
OOH*	-78.35	0.42	-0.22	-78.15
H*	-66.56	0.12	-0.017	-66.46

energies by -eU. The difference between the potential of a hole in the valence band of the catalytic substrate and the redox potential for O_2 evolution is basically the driving force for photocatalytic water oxidation, which was used to decide whether or not the reaction will proceed spontaneously upon irradiation of the sample[9]. This can be done by testing if each step in the free energy profile according to Eqs. (14-19) is downhill under the influence of the potential of a hole in the substrate valence band or, alternatively, by comparing the free energy of this hole with the reaction free energy of the water splitting reaction plus its associated overpotential. The latter is given by the difference between the potential needed for the overall reaction to be energetically neutral and the one causing every individual reaction step to be downhill in energy.

As shown in Fig. 8 (a-d), for monolayer β-GeSe, the potential of photogenerated electrons (U_e) and holes (U_h) for redox reactions is 1.27 V and 1.66 V at pH =0, respectively. According to the formula mentioned above, the corresponding U_e and U_h in a neutral solution (pH = 7) are 0.857 (1.27-0.059×7) and 2.073 (1.66+0.059×7) V respectively.

For monolayer β-SnSe shown in Fig. 8 (e-h), the potential of photogenerated electrons (U_e) and holes (U_h) for redox reactions is 1.29 V and 1.26 V at pH =0, respectively. And the corresponding U_e and U_h in a neutral solution (pH = 7) are 0.877 (1.29-0.059×7) and 1.673 (1.26+0.059×7) V respectively.

The intermediate steps are estimated by simulating the intermediate adsorption on a 2×2 supercell of the β-GeSe and β-SnSe monolayer. Different surface sites were examined by comparing the adsorption energy of OH^* and OOH^* to find the most favorable surface active site. As shown in Fig. S8, we have investigated six adsorption sites (1-4: top site, 5-6: bridge site) for the adsorption of OH^* and OOH^* for monolayer β-GeSe and β-SnSe. For
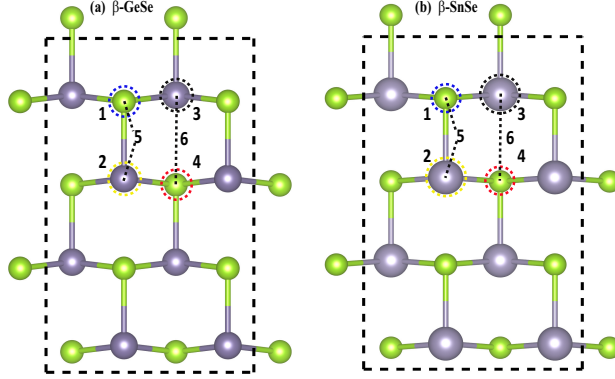
FIG. S8: The colored dashed circles indicate the OH^* and OOH^* adsorption sites of monolayer (a) β-GeSe and (b) β-SnSe

β-GeSe, after the geometrical optimization, we found that, the sites 4 and 6 do not support stable structures, and the most energetically stable adsorption structures are those with OH* and OOH^* on the in-plane germanium atoms. For monolayer β-SnSe, the OH^* is favorably adsorbed on the stannum atoms, while the OOH^* is favorably adsorbed on the bridge site between stannum and selenium atoms. Fig. 8(a) presents the atomic configurations of intermediates along the reaction pathway of water oxidation on the β-GeSe monolayer, and the corresponding free-energy profiles are summarized in Fig. 8 (c). The red lines in Fig. 8 (c) represent the situation without any external potential to simulate the condition without any light irradiation (U = 0) in a neutral solution. The water molecule is initially transformed into a OH^* species with a ΔG of 0.83 eV for water oxidation. Next, the OH^* species can be oxidized to be the O^* species by releasing an electron and a proton. Interestingly, this step release 0.047 eV. In the third step, a much higher free energy of 2.56 eV is required to oxidize O^* species to OOH^* species. Finally, the OOH^* species form a free O_2 molecule by releasing an electron and a proton, spontaneously. As a consequence, this step is exothermic by 0.07 eV in the free energy profile. Considering the irradiated sample in the neutral solution, the extra potential (U = 2.073 V) is provided by photogenerated holes, the third step is still uphill ($\Delta G = 0.49$ eV) shown as blue lines in Fig. 8 (c), indicating that the O^* species cannot be transformed into an OOH^* species spontaneously. However, the "all downhill" case (olive lines) starts from U = 2.57 V, in which all individual reaction steps are exergonic, and the overall reaction will proceed spontaneously without kinetic hindrance (assuming the absence of individual barriers for the reaction steps). According to this model, an additional external bias of 0.497 V (=2.57 - 2.073) would be needed to drive the whole

sequence at pH = 7, which is similar to that of FeNi@C (0.49 V)[10]. For monolayer β-SnSe as shown in Fig. 8 (c), the additional external bias of 0.287 V (=1.96 - 1.673) would be needed to drive the whole sequence at pH = 7, which is much lower than that of β-GeSe and also lower than that of Ni/graphene composite (0.35 V)[11], g-C_3N_4 (0.43 V)[12]. For both β-GeSe and β-SnSe, the calculated overpotentials are all lower than C_2N based type-II heterojunctions (C_2N/GaTe: 1.47 V, C_2N/InTe: 0.94 V)[13], many TM@C catalysts or metal oxides (0.49-1.7 V)[10] and the well-studied catalyst γ(Ni, Fe)OOH (0.56 V)[14].

For the hydrogen reduction half, there are only two steps, as displayed in Fig. 8 (b, d) and Fig. 8 (f, h). For the situation of pH = 0 without light irridiation (U = 0), firstly, the β-GeSe monolayer combines with a proton and an electron to form a $H*$ species with an unfavorable ΔG of 1.39 eV (1.44 eV for β-SnSe). Next, the H^* species continues to bond a proton and an electron to release a H_2 molecule, and finally the free energy reaches close to zero. Under the external potential (U=1.27 for β-GeSe and U=1.29 for β-SnSe) provided by photogenerated electrons, the first step for both cases is still uphill, but the barrier is obviously reduced (0.12 eV for β-GeSe and 0.15 for β-SnSe). However, the "all downhill" case (dotted olive line) start from U = 1.40 V and 1.45 V for β-GeSe and β-SnSe respectively. In other words, an additional external bias of (1.40 - 1.27) V= 0.13 V for β-GeSe and (1.45 - 1.29) V= 0.16 V for β-SnSe would be needed to drive the whole sequence at pH = 0.

———————

[1] J. Bardeen and W. Shockley. Deformation potentials and mobilities in non-polar crystals. Physical Review, 80:72–80, 1950.

[2] Yu Wu, Ke Xu, Congcong Ma, Ying Chen, Zixuan Lu, Hao Zhang, Zhilai Fang, and Rongjun Zhang. Ultrahigh carrier mobilities and high thermoelectric performance at room temperature optimized by strain-engineering to two-dimensional aw-antimonene. Nano Energy, 63, SEP 2019.

[3] Bo Peng, Hao Zhang, Hezhu Shao, Ke Xu, Gang Ni, Jing Li, Heyuan Zhu, and Costas M. Soukoulis. Chemical intuition for high thermoelectric performance in monolayer black phosphorus, a-arsenene and aw-antimonene. Journal of Materials Chemistry A, 6(5):2018–2033, 2018.

[4] Lin Ju, Jing Shang, Xiao Tang, and Liangzhi Kou. Tunable photocatalytic water splitting

by the ferroelectric switch in a 2d agbip$_2$se$_6$ monolayer. Journal of the American Chemical Society, 142(3):1942–1500, 2020.

[5] Shiyou Chen and Linwang Wang. Thermodynamic oxidation and reduction potentials of photocatalytic semiconductors in aqueous solution. Chemistry of Materials, 24(18):3659–3666, 2012.

[6] D. R. Lide. Crc handbook of chemistry and physics, 84th edition. CRC Press: Boca Raton, FL,, 2003-2004.

[7] Jens K Norskov, Jan Rossmeisl, Logadottir, A, L Lindqvist, John R Kitchin, Thomas Bligaard, and Hannes Jonsson. Origin of the overpotential for oxygen reduction at a fuel-cell cathode. Journal of Physical Chemistry B, 108(46):17886–17892, 2004.

[8] NIST Computational Chemistry Comparison and Benchmark Database, NIST Standard Reference Database Number 101, Release 19, April 2018, edited by Russell D. Johnson, III, Available at http:// cccbdb.nist.gov/.

[9] G. J. Kroes. Oxidation and photo-oxidation of water on tio2 surface. Journal of Physical Chemistry C, 112(26):9872–9879, 2008.

[10] Xiaoju Cui, Pengju Ren, Dehui Deng, Jiao Deng, and Xinhe Bao. Single layer graphene encapsulating non-precious metals as high-performance electrocatalysts for water oxidation. Energy Environ. Sci., 9:123–129, 2016.

[11] Guoping Gao, Steven Bottle, and Aijun Du. Understanding the activity and selectivity of single atom catalysts for hydrogen and oxygen evolution via ab initial study. Catal. Sci. Technol., 8:996–1001, 2018.

[12] Jonas Wirth, Rainer Neumann, Markus Antonietti, and Peter Saalfrank. Adsorption and photocatalytic splitting of water on graphitic carbon nitride: a combined first principles and semiempirical study. Phys. Chem. Chem. Phys., 16:15917–15926, 2014.

[13] Xu Zhang, An Chen, Zihe Zhang, Menggai Jiao, and Zhen Zhou. Rational design of c$_2$n-based type-ii heterojunctions for overall photocatalytic water splitting. Nanoscale Adv., 1:154–161, 2019.

[14] Daniel Friebel, Mary W. Louie, Michal Bajdich, Kai E. Sanwald, Yun Cai, Anna M. Wise, Mu-Jeng Cheng, Dimosthenis Sokaras, Tsu-Chien Weng, Roberto Alonso-Mori, Ryan C. Davis, John R. Bargar, Jens K. Nørskov, Anders Nilsson, and Alexis T. Bell. Identification of highly active fe sites in (ni,fe)ooh for electrocatalytic water splitting. Journal of the American

Chemical Society, 137(3):1305–1313, 2015.